Intramolecular Charge Transfer Assisted by Conformational Changes in the Excited State of Fluorene-dibenzothiophene-*S*,*S*-dioxide Co-oligomers

Fernando B. Dias,* Sam Pollock, Gordon Hedley, Lars-Olof Pålsson, and Andy Monkman

OEM Research Group, Department of Physics, University of Durham, Durham DH1 3LE, U.K.

Irene I. Perepichka,† Igor F. Perepichka,‡ Mustafa Tavasli, and Martin R. Bryce

Department of Chemistry, University of Durham, Durham DH1 3LE, U.K.

Received: July 11, 2006

The strong solvatochromism observed for two fluorene-dibenzothiophene-*S*,*S*-dioxide oligomers in polar solvents has been investigated using steady-state and time-resolved fluorescence techniques. A low-energy absorption band, attributed to a charge-transfer (CT) state, is identified by its red shift with increasing solvent polarity. In nonpolar solvents, the emission of these conjugated luminescent oligomers shows narrow and well-resolved features, suggesting that the emission comes from a local excited state (LE), by analogy to their conjugated fluorene-based polymer counterparts. However, in polar solvents, only a featureless broad emission is observed at longer wavelengths (CT emission). A linear correlation between the energy maximum of the fluorescence emission and the solvent orientation polarizability factor Δf (Lippert−Mataga equation) is observed through a large range of solvents. In ethanol, below 230 K, the emission spectra of both oligomers show dual fluorescence (LE-like and CT) with the observation of a red-edge excitation effect. The stabilization of the CT emissive state by solvent polarity is accompanied/followed by structural changes to adapt the molecular structure to the new electronic density distribution. In ethanol, above 220 K, the solvent reorganization occurs on a faster time scale (less than 10 ps at 290 K), and the structural relaxation of the molecule ($CT_{unrelaxed} \rightarrow CT_{Relaxed}$) can be followed independently. The magnitude of the forward rate constant, $k_1(20\ ^\circ C) \approx 20 \times 10^9\ s^{-1}$, and the reaction energy barrier, $E_a \approx 3.9$ kcal mol^{-1}, close to the energy barrier for viscous flow in ethanol (3.54 kcal mol^{-1}), show that large-amplitude molecular motions are present in the stabilization of the CT state.

I. Introduction

After more than 15 years since the discovery of electroluminescence in conjugated luminescent polymers,[1] there is intense activity in this field combining applied and fundamental research.[2−4] Conjugated polymers are the key component of solid-state devices, promising a truly disruptive technology in the forthcoming years.[5,6] The potential applications of these materials due to their semiconductor characteristics[3,7] are enormous, embracing passive and active matrix displays, electronic devices, biochemical sensing, and lighting.[5,6,8,9]

Among the large class of semiconductive organic conjugated polymers, polyfluorenes (PFs) and fluorene-based copolymers are the most promising for electroluminescent applications.[4,5,10] The strong blue emission, excellent thermal and chemical/electrochemical stability, and the possibility of tuning the emission across the entire visible spectrum by appropriate chemical modification are their main advantages.

Besides the excellent optical properties and suitable HOMO/LUMO energy levels, PFs possess great charge-transport properties, with hole mobilities of more than 1 order of magnitude higher than that in poly(*p*-phenylenevinylene) (PPV).[11] However, the mobility and injection of electrons are much lower than those of holes; thus, the transport of positive and negative carriers is greatly unbalanced.[12] Another major problem in polyfluorene materials is the formation of fluorenone defects as a result of thermal-, photo-, or electrical degradation, which is frequently encountered in these materials, resulting in low-energy emission bands.[13] Many different approaches have been used to mitigate these problems; among them is the introduction of either electron donor or electron acceptor moieties into the homopolymers (in the backbone, as side chains or endcaps).[14] However, copolymerization leads to materials with either different spectroscopic properties or different charge and excited-state mobilities, which are affected by the relative order of the monomers' frontier energy levels. The photoluminescence and the electroluminescence depend not only on the nature of the copolymer units but also on their arrangement along the polymer backbone. Conjugated alternating donor−acceptor-type copolymers generally show single photoluminescence bands,[15] whereas random copolymers have a tendency to show dual emission from wider and narrower band gap domains[16] although dual photoluminescence of alternating fluorene copolymers in solution has been recently reported.[17]

Although diverse copolymers have been developed to tune the emission color, systematic studies on the effects of incorporating different monomer units into oligo- or polyfluorene

* To whom correspondence should be addressed. E-mail: f.m.b.dias@durham.ac.uk.

† Visiting student from Donetsk National University, Ukraine. Current address: Department of Chemistry, University of Montreal, Montreal, Quebec H3C 3J7, Canada.

‡ On leave from L. M. Litvinenko Institute of Physical Organic and Coal Chemistry, National Academy of Sciences of Ukraine, Donetsk 83114, Ukraine.

10.1021/jp0643653 CCC: $33.50
Published on Web 09/02/2006

CHART 1

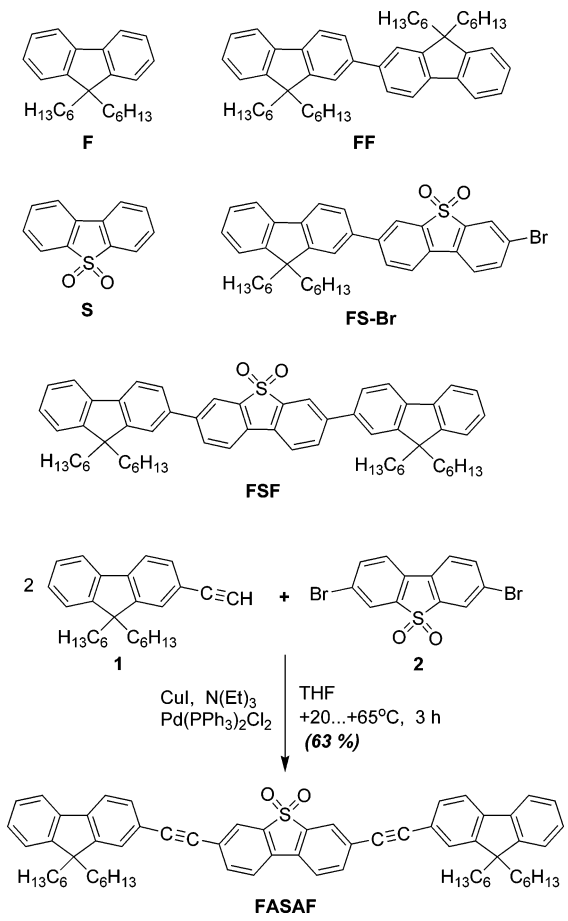

chains are still lacking. This approach can give valuable insights into fundamental aspects of the physics involved in these systems and can also provide guidelines to develop new strategies for practical applications.

Recently, we reported the synthesis of fluorene-dibenzothiophene-*S*,*S*-oxide co-oligomers, which possess improved electron affinity and stability toward both p- and n-doping and retain high photoluminescence (PL) efficiency in both solution and solid state.[18]

The aim of the present work was to probe deeper into the photophysical processes that occur in these materials and thereby enhance their potential for further structural modification and exploitation. Our studies focus on the fluorene-dibenzothiophene-*S*,*S*-dioxide oligomers **FSF** and **FASAF** (Chart 1). This study establishes that incorporation of the dibenzothiophene-*S*,*S*-dioxide unit into the fluorene oligomers leads to dual fluorescence, suggesting that fluorescence emission occurring from two relaxed singlet excited states is dependent on the solvent polarity and temperature. We demonstrate that a fast intramolecular charge transfer (CT) to the electron-deficient **S** moiety, stabilized by the polar solvent and accompanied/followed by structural reorganization of the molecule (in the excited state), is the origin of the broad, featureless emission from these systems, by direct analogy to molecular systems that show twisting or planarization of the excited state by intramolecular charge transfer (TICT or PICT, respectively).[19]

II. Experimental Section

Dibenzothiophene-*S*,*S*-dioxide (**S**) was obtained by oxidation of commercial dibenzothiophene by H_2O_2 in acetic acid, similar to literature procedures[20] (a scale-up synthesis is given in Supporting Information). Dihexylfluorene (**F**) was obtained by alkylation of fluorene by 1-bromohexane using the procedure described for 2,7-dibromofluorene.[18] 9,9,9′,9′-Tetrahexyl-2,2′-bifluorene (**FF**) was obtained in a fashion similar to literature procedures[21] (see Supporting Information). The dimer **FS**−**Br**[18] and the trimer **FSF**[18] have been prepared as described previously.

3,7-Bis-(9,9-dihexyl-2-ethynylfluorene)-dibenzothiophene-*S*,*S*-dioxide (FASAF). To a solution of 9,9-dihexyl-2-ethynylfluorene (**1**)[22] (0.81 g, 2.26 mmol) and 3,6-dibromodibenzothiophene-*S*,*S*-dioxide (**2**) (0.42 g, 1.13 mmol) in anhydrous tetrahydrofuran (THF) (15 mL) under argon, CuI powder (dried in vacuo at 250 °C) (7 mg, 0.04 mmol) and dry triethylamine (0.5 mL) were added, and the reaction mixture was stirred at room temperature for 20 min. $Pd(PPh_3)_2Cl_2$ catalyst (0.022 g, 0.03 mmol) was added in one portion, resulting in brown coloration, and the mixture was stirred under argon at room temperature for 1 h, followed by reflux (oil bath, 65 °C) for another 2 h. The mixture was cooled to room temperature, filtered to remove inorganic solids, and washed with THF, and the solvent was removed in vacuo, affording the crude product **FASAF** (1.05 g) as a light-brown powder. It was twice purified by flash chromatography on silica gel (column 5 cm × 20 cm) using dichloromethane (DCM)−petroleum ether (1:1 v/v) as the eluent to yield analytically pure **FASAF** (0.66 g, 63%) as a bright-yellow powder, mp 181−183 °C. ^{1}H NMR (400 MHz, $CDCl_3$): δ 8.01 (2H, d, J = 1.6 Hz, **S**−H4), 7.81 (2H, dd, J = 1.6 and 8.0 Hz, **S**−H2), 7.78 (2H, d, J = 8.0 Hz, **S**−H1), 7.73−7.69 (4H, m), 7.56−7.52 (4H, m), 7.38−7.33 (6H, m), 1.99 (8H, t, J = 8.2 Hz, $CH_2C_5H_{11}$), 1.15−1.00 (24H, m, $(CH_2)_2$-$(CH_2)_3CH_3$), 0.77 (12H, t, J = 7.0 Hz, CH_3), 0.66−0.56 (8H, m, $CH_2CH_2C_4H_9$). ^{13}C NMR (75 MHz, $CDCl_3$): δ 151.17, 150.97, 142.31, 140.21, 138.42, 136.69, 130.89, 130.13, 127.81, 126.97, 126.31, 126.17, 125.14, 122.96, 121.65, 120.32, 120.17, 119.78, 94.74, 87.63, 55.22, 40.36, 31.51, 29.70, 23.75, 22.59, 13.99. EIMS *m*/*z*: 928 (M^+, 100%), 929 (M^+, 68.63%), 930 (M^+, 30.70%). Anal. Calcd for $C_{66}H_{72}O_2S$ (MW = 929.34): C, 85.30; H, 7.81; S, 3.45. Found: C, 84.81; H, 7.77; S, 3.54.

All the compounds were studied using dilute solutions with an optical density below 0.2 at the maximum absorption wavelength, corresponding to concentrations of $\sim 10^{-6}$ mol L^{-1}. Super purity grade solvents were purchased from ROMIL and used as supplied: hexane (Hx, $\Delta f = 0.093$), methylcyclohexane (MCH, $\Delta f = 0.1$), dioxane (Dx, $\Delta f = 0.127$), toluene (Tol, $\Delta f = 0.13$), anisole (An, $\Delta f = 0.232$), chloroform (CHF, $\Delta f = 0.255$), chlorobenzene (CHB, $\Delta f = 0.263$), 1,2-dichlorobenzene (DCB, $\Delta f = 0.31$), dichloromethane (DCM, $\Delta f = 0.319$), benzonitrile (BzN, $\Delta f = 0.353$), acetone (AC, $\Delta f = 0.375$), *N*,*N*-dimethylformamide (DMF, $\Delta f = 0.377$), ethanol (EtOH, $\Delta f = 0.379$), acetonitrile (ACN, $\Delta f = 0.392$), and methanol (MeOH, $\Delta f = 0.393$). Absorption spectra were obtained using a Perkin-Elmer Lambda 19 double-beam spectrophotometer in 1 cm path length quartz cells. Steady-state photoluminescence spectra were recorded on a Fluorolog fluorescence spectrometer (Jobin Yvon) with double-excitation double-emission monochromators using a right angle configuration. Time-resolved fluorescence decays were collected using the picosecond time correlated single photon counting technique (impulse response function, IRF = 24 ps). The excitation source, with vertical polarization, was a picosecond Ti:sapphire laser from Coherent Inc. (wavelength range: 720 to 1000 nm, 76 MHz repetition rate), coupled to a second harmonic generator (360 to 500 nm). Emission collected at magic angle polarization was detected through a SpectraPro-2300i double subtractive monochromator (Acton Research

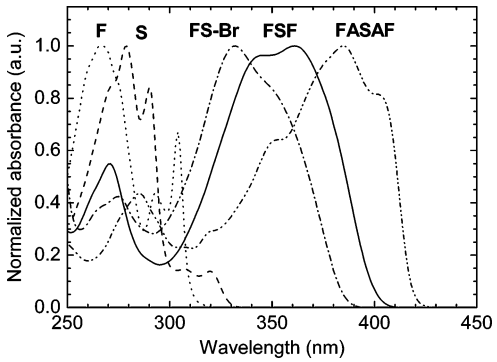

Figure 1. Absorption spectra of **F**, **S**, **FS**−**Br**, **FSF**, and **FASAF** in MCH.

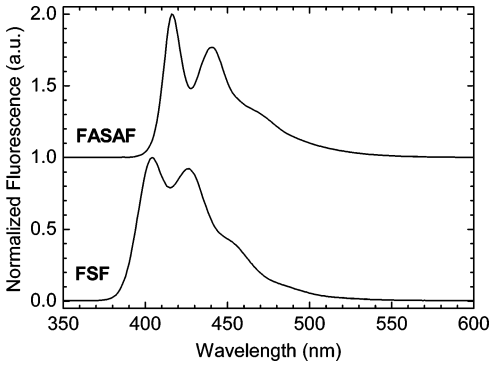

Figure 2. Emission spectra of **FSF** and **FASAF** in MCH, $\lambda_{ex} = 385$ nm.

Corporation) by a Hamamatsu model R3809U-50 microchannel plate (MCPT). Signal acquisition was performed using a TCSPC module from Becker & Hickl (model SPC-630) using 4096 channels on a 0.8 ps/channel time scale. Deconvolution of the fluorescence decays was performed using the Globals WE software package.[23] Random flat residuals between [−2, 2] were obtained in all cases with χ^2 values close to unity (see Figure S1 in Supporting Information). Fluorescence decays collected as a function of temperature were acquired using a model VNF-100 cryostat from Janis Research Inc. Time-resolved spectra were acquired using a model C5680 streak camera from Hamamatsu having a 10 ps IRF.

III. Results and Discussion

A. Steady-State Photoluminescence. *Absorption and Emission Spectra in a Methylcyclohexane Solution.* Figure 1 shows the absorption spectra of compounds **F**, **S**, **FS**−**Br**, **FSF**, and **FASAF** in a methylcyclohexane (MCH) solution. The spectrum of **F** shows a broad band centered around 270 nm and two well-resolved peaks at 292 and 304 nm. The **S** spectrum displays a more structured primary absorption band with two main components at 279 and 290 nm; again, similar to **F**, two minor peaks are seen at longer wavelengths (308 and 320 nm). When **F** and **S** are coupled in **FS**−**Br**, **FSF**, or **FASAF**, the absorption spectra show a marked difference. Together with the band at 275 nm, a new broad absorption band is observed between 300 and 380 nm for **FS**−**Br**, 300 and 400 nm for **FSF**, and 300 and 420 nm for **FASAF**. This broad band is not seen in either **F** or **S**, showing that the coupling of these units induces a strong interaction between them, assigned to the excitation delocalized through all of the units in **FS**−**Br**, **FSF**, and **FASAF**. Similar conclusions were obtained from quantum chemical characterization of fluorene-based copolymers containing benzothiadiazole units.[24] The shift to longer wavelengths observed in **FASAF**, relative to **FSF**, suggests an increase in the conjugation level of the π orbitals for **FASAF**.

Emission spectra of **FSF** and **FASAF** in MCH solution are shown in Figure 2. In both cases, the emission did not change upon varying the excitation wavelength (see Figure S2 in Supporting Information). Note also the excellent match between the excitation spectra collected at 410 and 550 nm at 290 K (Results and Discussion and Figure 7a) and the absorption spectrum. The smaller Stokes shift (0.24 vs 0.36 eV) and better vibronic structure for **FASAF** compared with those for **FSF** indicate a greater similarity between the ground- and excited-state structures in **FASAF**, and the red shift observed in fluorescence for **FASAF** (compared with **FSF**) suggests extended conjugation in this longer oligomer.

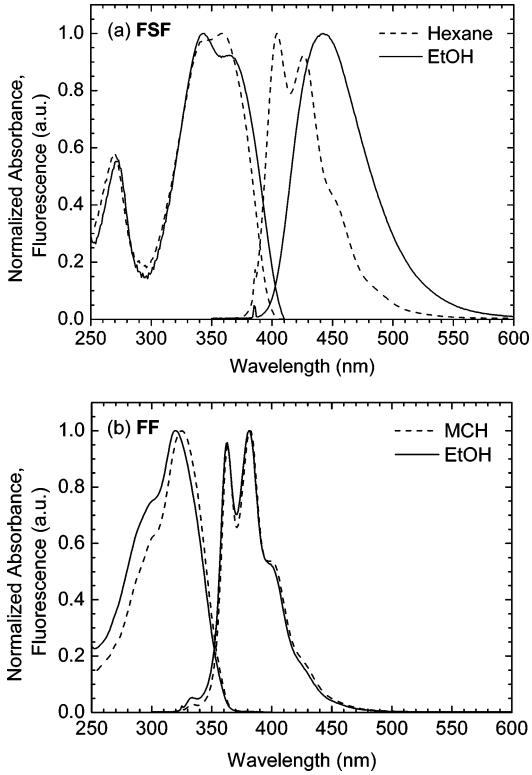

Figure 3. Normalized absorption and emission spectra of (a) **FSF** in hexane and ethanol and (b) **FF** in methylcyclohexane and ethanol solutions. ($\lambda_{abs} = 330$ nm (dichloromethane) and $\lambda_{PL} = 370$ nm (chloroform) for **FF** have been reported,[26] but no spectra have been presented).

Solvatochromic Measurements. Spectral changes induced by solvent polarity are exemplified by comparison of the absorption and emission (PL) spectra for **FSF** in hexane (dielectric permittivity $\epsilon = 1.89$) and ethanol ($\epsilon = 24.3$) (Figure 3a). In the more polar solvent (ethanol), the absorption spectrum of **FSF** shows minor changes compared with the spectrum in hexane. However, a slight red shift is clearly observed on the red-edge side of the main absorption band. This red shift, also observed for **FASAF** but to a lesser degree, is consistent with the increase in the solvent polarity (Figure S3 in Supporting Information) and is not present in the absorption spectrum of the dimer, 2,2′-bi(9,9-dihexylfluorene) (**FF**) (Figure 3b), strongly suggesting the presence of a low-energy CT band in the absorption spectra of **FSF** and **FASAF**. A similar behavior was observed for *p*-antryl and *p*-acridyl derivatives of *N*,*N*-dimethylaniline.[25]

The changes in the emission spectra are more pronounced: in hexane, a well-structured progression is observed with the

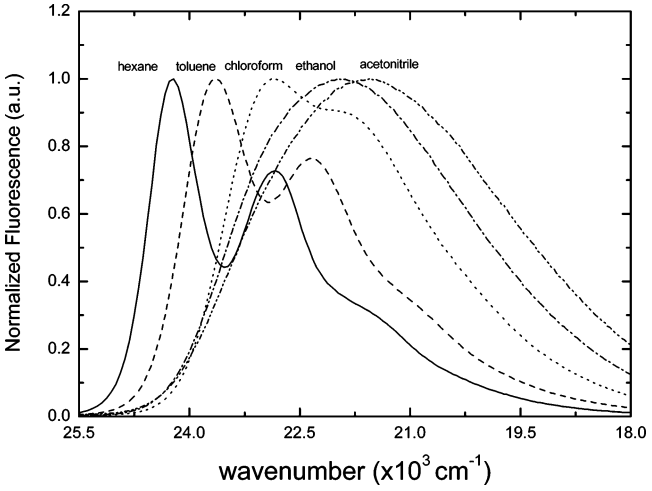

Figure 4. Solvatochromic shift of the emission spectrum of **FASAF** in solvents with different orientation polarizability Δf (see Experimental Section).

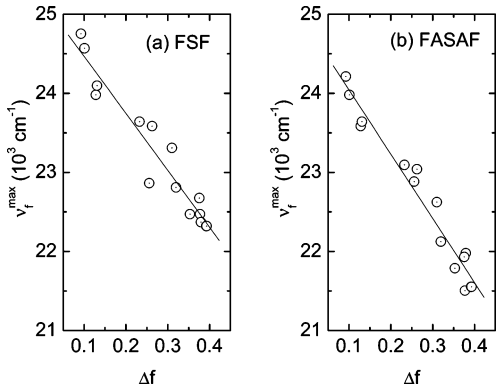

Figure 5. Solvatochromic shift of the emission maximum, ν_{max}, for (a) **FSF** and (b) **FASAF** against the solvent polarity parameter (Lippert−Mataga equation; see the text). The solvents and their Δf values are given in the Experimental Section.

maximum intensity at 404 nm, and in ethanol, the vibronic structure in PL is lost with a pronounced red shift to 445 nm. All of these effects are absent in the absorption and emission spectra of **FF**, as follows from its spectra in MCH ($\epsilon = 2.02$) and ethanol (Figure 3b), giving evidence of the important role of the dibenzothiophene-*S*,*S*-dioxide unit **S** in the solvatochromism in **FSF** and **FASAF** (Figure 3a).

Ground-state dipole moments were determined for **F** (0.36 D), **FFF** (0.17 D), **S** (5.5 D), and **FSF** (5.7 D) using density functional theory (DFT) calculations in the gas phase. Despite the strong dipole moment of **S** when compared with that of **F** or **FFF**, no significant solvatochromic shift is observed for **S**, showing once more that the strong solvatochromism evidenced by **FSF** and **FASAF** is due to the presence of a charge-transfer process between **F** (donor) and **S** (acceptor) units.

To study in more detail the solvatochromism evidenced by **FSF** and **FASAF**, the fluorescence spectrum of each compound was collected in various solvents with different polarities and polarizabilities (see Figures 4 and 5).

The plots of the emission maxima, ν_{max}, of **FSF** and **FASAF** as a function of the solvent orientation polarizability parameter, $\Delta f = (\epsilon - 1)/(2\epsilon + 1) - 1/2((n^2 - 1)/(2n^2 + 1))$ (Lippert−Mataga equation[19,25]), showed a reasonably good linear relationship (correlation coefficients 0.96 and 0.98 for **FSF** and **FASAF**, respectively), with a decrease in the energy of the emission maximum with an increase in Δf (Figure 5a, b), showing that the excited-state dipole moment is larger[19,25,27] for both **FSF** and **FASAF** compared to their ground-state dipole moments. Note that no significant differences were found between protic and aprotic solvents, showing that hydrogen bonding is not responsible for the observable red shift.

Spectral changes in the emission spectra with the occurrence of dual fluorescence as a function of solvent polarity have been explained in small molecules such as 4-(dimethylamino)-benzonitrile (DMABN) and related compounds by the presence of two different excited states that are closely spaced in energy (i.e., a local excited state (LE) mainly emitting in nonpolar solvents and an intramolecular charge-transfer state (CT) mainly emitting in polar solvents[19,27,28]). Depending on the polar solvent reorientation during the lifetime of the fluorophore excited state, an inversion of the energy order of the two states takes place, turning the CT into the lowest excited state. Since this first explanation was proposed by Lippert,[19] other hypotheses have been advanced to explain the phenomenon (i.e., the occurrence of dual fluorescence). Among them, there are the "twisting mechanism", TICT,[19] assuming that the molecule is capable of internal rotation, leading to a 90° twist between the donor and acceptor units in the final equilibrated CT state, and the "planar mechanism", PICT,[19,27,28] which assumes that in polar solvents the S_2 state with the larger dipole moment becomes the lowest excited state in a dynamic state inversion controlled by the small energy gap between the two lowest excited singlet states (S_1 and S_2). (In this model, the final structure of the equilibrated CT state is postulated to be planar.)

For large π-electronic D−A systems such as *p*-antryl and *p*-acridyl derivatives of *N*,*N*-dimethylaniline,[19,25,29] strong coupling between the LE and CT states was also used to interpret the spectroscopic observations; the relative contribution of both states to the wave function of the relaxed emissive CT state is dependent on the solvent polarity, which controls the energy gap between the LE and CT states. For example, in the case of 4-(9-acridyl)julolidine, a shift from LE-like to CT-like emission is observed on going from nonpolar to polar solvents.[25] An indication that the average twist angle between donor and acceptor units in the emissive CT state increases with solvent polarity was also found.[19,25]

For **FSF** and **FASAF**, the emission spectra profile observed in solvents with intermediate Δf values (Figure 4 and Figure S4 in Supporting Information) suggest a dual fluorescence spectrum (LE/CT). However, consistent with what happens with the *N*,*N*-dimethylaniline derivatives referred to above, strong electronic coupling between the LE and CT states in nonpolar solvents can also explain the evolution of the emission profile;[25] increasing the solvent polarity increases the energy gap between the LE and CT states and decreases the relative contribution of the LE to the wave function of the emissive state, leading in the more polar solvents to a spectroscopic signature with mainly CT character. The observation of a linear correlation over the whole range of solvents in Figure 5a and b suggesting a similar dipole moment for the emissive state in polar and nonpolar solvents gives additional support to this scenario.

Temperature Effect on the Emission Spectra of FSF and FASAF in Ethanol. The steady-state emission spectra of **FSF** and **FASAF** in an ethanol solution, obtained as a function of temperature, are presented in Figure 6. Above 230 K, both compounds show broad spectra similar to those observed at room temperature with only a slight increase in the emission intensity with decreasing temperature (Figure 6a, c). Below 230 K, the broad emission is blue shifted to a more resolved

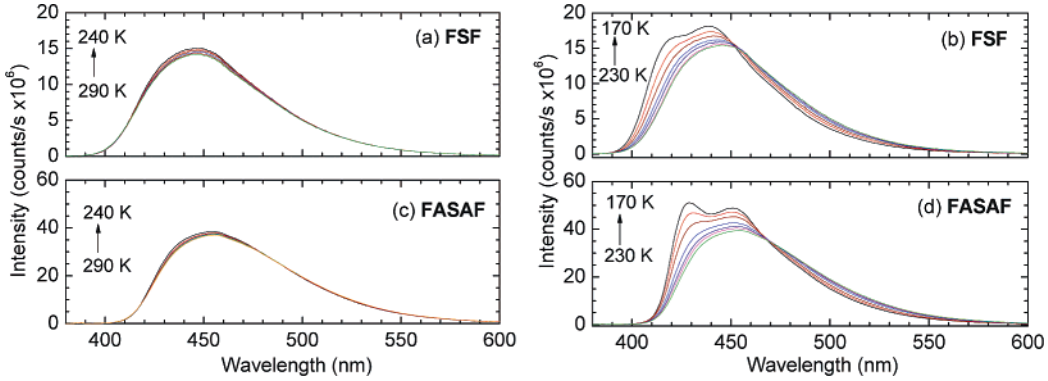

Figure 6. Temperature dependence of (a, b) **FSF** and (c, d) **FASAF** emission spectra in ethanol. Isoemissive points are clearly observed below 230 K for both compounds.

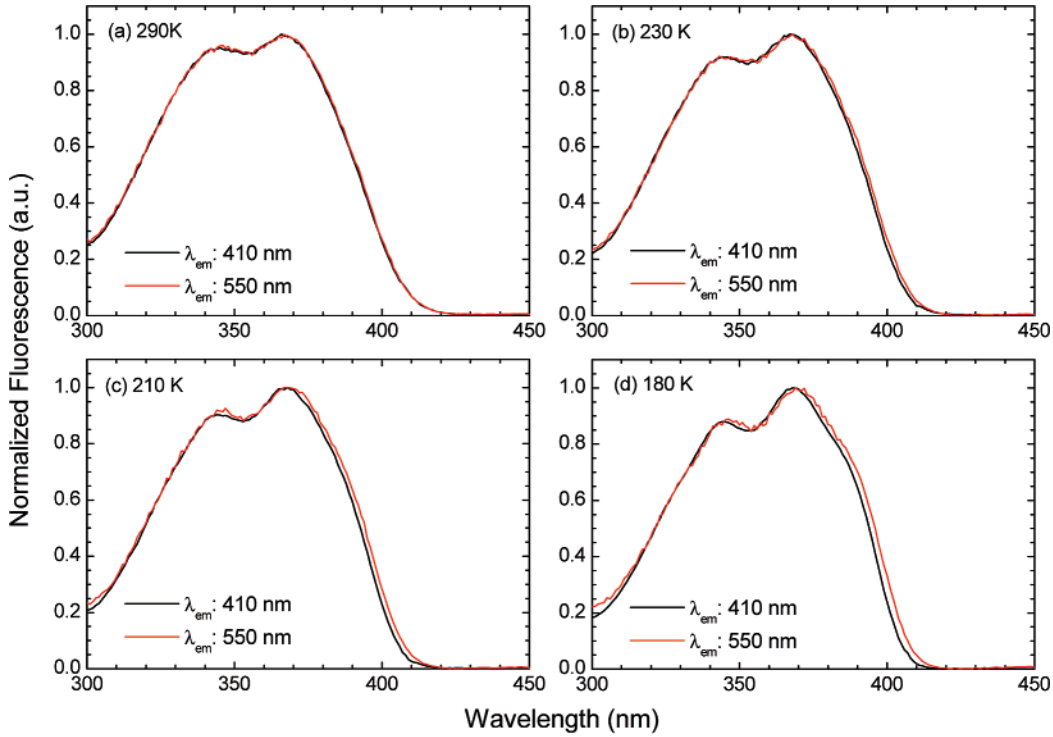

Figure 7. Excitation spectra of **FSF** in ethanol, collected at 410 nm (black) and 550 nm (red).

spectrum similar to that obtained in nonpolar solvents, with clear isoemissive points for both **FSF** and **FASAF** at 453 and 468 nm, respectively (Figure 6b, d). Despite the strong spectral overlap between these emission spectra, the observation of the isoemissive points indicates the presence in both cases of two different fluorescent species, suggesting that the broad emission band (CT-like) is formed at the expense of the more structured emission (LE-like).

Dependence of the Excitation Spectra of FSF and FASAF in Ethanol on the Emission Wavelength. Identical excitation spectra for **FSF** and **FASAF** were obtained between 300 and 450 nm at 290 K for two different emission wavelengths (410 and 550 nm, Figure 7a), showing that the emission of both compounds is independent of the excitation wavelength at room temperature in the spectral range considered. Decreasing the temperature induces a small but significant wavelength dependence on the excitation spectra of both compounds. (Note that this is equivalent to saying that the emission spectra of both compounds are dependent on the excitation wavelength.) The red shift is observed only for excitation on the long-wavelength edge of the absorption band, with no changes in the shape of the spectra, and is observed only for temperatures below 230 K (Figure 7b–d), with the excitation spectra collected at 550 nm showing a gradual broadening to longer wavelengths relative to that collected at 410 nm (by ~2 nm at 180 K).

This unusual behavior has been described before as a red-edge excitation effect (REE) occurring as a consequence of solute–solvent interactions,[30,31] which induces an inhomogeneous broadening of the energy levels. Because the fluorophore dipole moments are different in the ground and excited states, when the excited-state radiative decay starts to compete with the solvent relaxation time, excitation at low energies would select mainly those chromophores with a solvent configuration equivalent to that of the final relaxed state.[31] Thus, the observation of a REE effect should be prominent when (i) excitation leads to a large change in the dipole moment and (ii) the solvent relaxation time increases.[31]

For **FSF** and **FASAF**, because the relative contribution of the LE state to the emissive state depends on the solvent reorganization, the presence of a REE below 230 K explains the appearance of the structured emission below that temperature; simply the reorganization of the solvent around the fluorophore is sufficiently slow to allow the competition of the radiative decay from a state with a relatively larger contribution

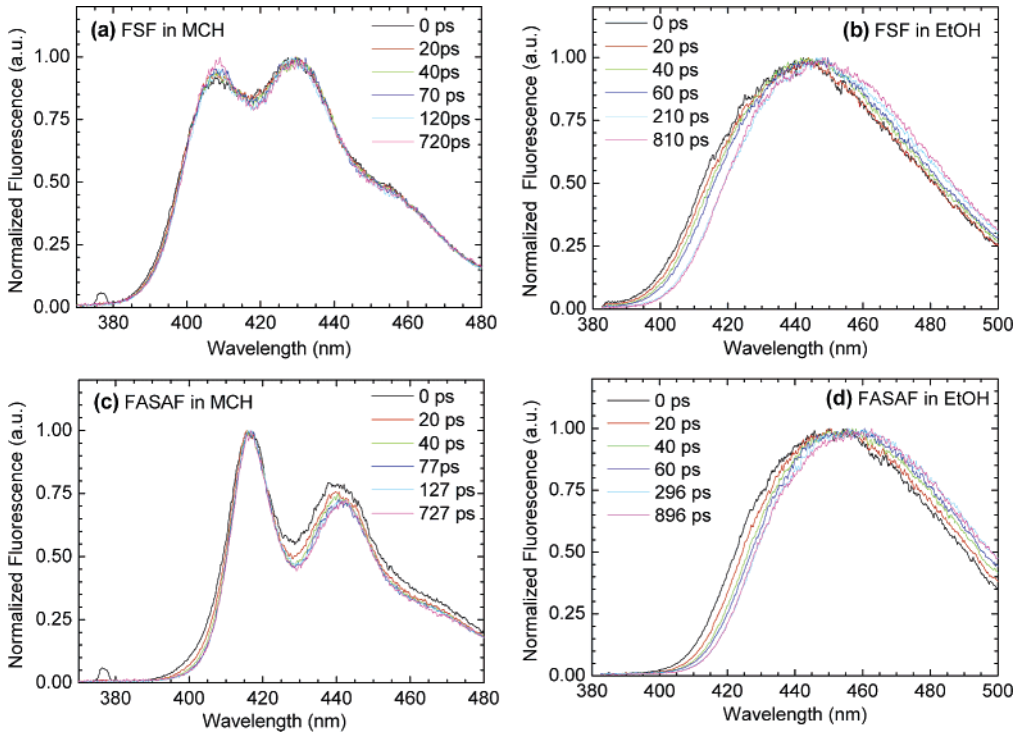

Figure 8. Time-resolved emission spectra of (a, b) **FSF** and (c, d) **FASAF** in (a, c) MCH and (b, d) ethanol normalized to 1 independently of the emission wavelength (see Figure S6 in Supporting Information for expanded spectra at the isoemissive points).

of the LE state. As a consequence, the fluorescence lifetimes of **FSF** and **FASAF** below 230 K are expected to be dependent on the emission wavelength.

B. Time-Resolved Photoluminescence. *Time-Resolved Emission Spectra at Room Temperature.* Time-resolved emission spectra of **FSF** and **FASAF** in MCH and ethanol solutions, normalized to 1 independently of the emission wavelength, are presented in Figure 8. In the nonpolar solvent (MCH), no significant spectral changes are observed for **FSF** in a time window up to 720 ps (Figure 8a). However, for **FASAF**, changes in the relative intensities and spectral narrowing of the two vibronic bands are observed in the first 40 ps, showing a decrease in the emission intensity with time on the blue side of both bands (Figure 8c). Similar behavior previously observed for poly[9,9-bis(2′-ethylhexyl)fluorene] (PF2/6) in MCH solution was interpreted as arising from conformational relaxation of the polymer backbone in the excited state.[32] Fluorescence decays of PF2/6 collected at the emission onset and tail fit a biexponential description with a fast component (40 ps) appearing as a decay time on the emission onset and as a build-in at longer wavelengths. For **FASAF**, an emission increase at longer wavelengths is not clearly observed with time (see Figure 8c). However, if the fractional contribution of the process is negligible, it could be easily hidden by the normalization, particularly if the spectra are affected by noise. In fact, when an expansion of the **FASAF** time-resolved spectrum is obtained and the emission is collected with better spectral resolution (Figure S5 in Supporting Information), an increase in the fluorescence emission with time is observed on the red side of the first vibronic band, being much less pronounced in the second vibronic.

In ethanol, both **FSF** and **FASAF** emission spectra show marked changes with time in the first 60−80 ps (Figure 8b, d). The emission intensities decrease on the blue side of the emission spectra and increase on the red side with the observation of isoemissive points (at ∼445 and 455 nm for **FSF** and **FASAF**, respectively), suggesting that the spectral changes observed in ethanol are not the result of simple continuous spectral relaxation but are rather the signature of two different species that are kinetically related. (Note that all of the spectra were normalized to 1 independently of the emission wavelength; thus, the isoemissive points are not artificially introduced.) Interestingly, emission from the LE-like state is not observed on the $t > 10$ ps time scale (Figure 8b, d), showing that the reorganization of the polar solvent is complete after 10 ps and suggesting that the spectral evolution observed in Figure 8b and d is not the result of solvent reorganization but is instead due to a conformational change of the molecule to adapt the structure to a new electron density distribution.

The similarity between the emission spectra of **FSF** and **FASAF** in nonpolar solvents and the emission spectrum of fluorene-based polymers with a fully planar structure[32] strongly suggests a quasi-planar conformation for the LE state. In this scenario, the conformational change referred to above could be an increase in the average twist angle between the **F** and **S** units to stabilize the emissive CT state in a perfect analogue to a TICT state.

Time-Resolved Fluorescence Decays at Room Temperature. Time-resolved fluorescence decays of **FSF** and **FASAF** were carried out in dilute MCH and ethanol solutions at room temperature, with an excitation wavelength of 395 nm and emission collected at several wavelengths. Single-exponential fluorescence decays were obtained for **FSF** in MCH, independent of the emission wavelength, with a decay time of 1.03 ns. For **FASAF**, the fluorescence decays in MCH are bi-exponential with decay times of 37 and 780 ps. (See Figure 9a, c and Table 1.) The faster decay component appears as a decay time (positive amplitude) on the emission onset and as a rise time (negative amplitude) at longer wavelengths. However, in agreement with the observation made from the time-resolved spectra, the fractional weight of the faster component is low and decreases at longer wavelengths (Table 1).

In the polar solvent (ethanol), more complex decays were obtained for both **FSF** and **FASAF** (Figure 9b, d and Table 1).

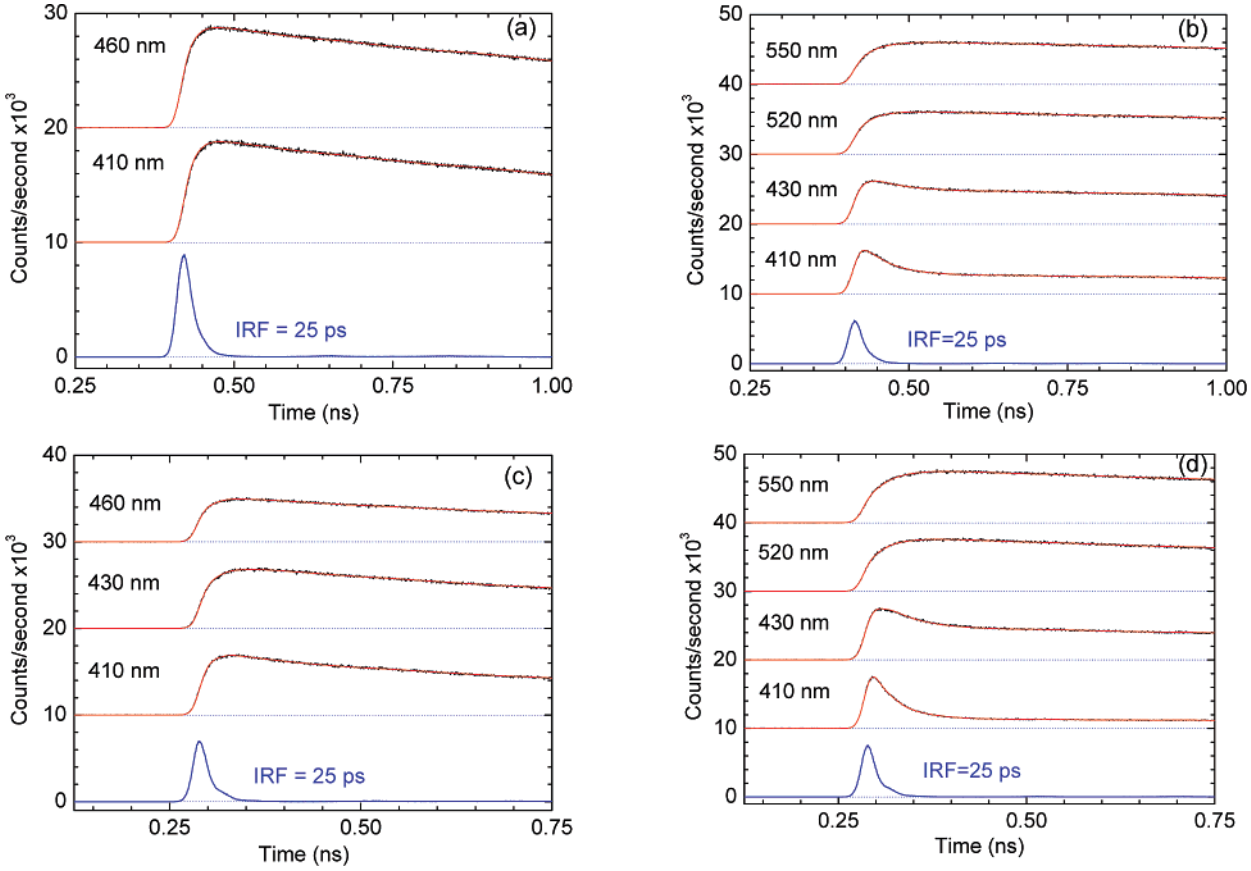

Figure 9. Independent single-wavelength analysis of (a, b) **FSF** and (c, d) **FASAF** fluorescence decays collected at different emission wavelengths. (a) Single-exponential fit of **FSF** fluorescence decay in MCH, (b) two-exponential fit of **FSF** fluorescence decay in ethanol, (c) two-exponential fit of **FASAF** in MCH, (d) two-exponential fit of **FASAF** in ethanol [experimental data (black lines) and fits (red lines)]. $\lambda_{ex} = 395$ nm. Note: the decays collected at 410 nm, both for **FSF** and **FASAF** in ethanol, are best fitted with sums of three-exponential functions (see Table 1 and Figure S7 in Supporting Information).

TABLE 1: τ_i, A_i, and χ^2 Values from Time-Resolved Fluorescence Decays of FSF and FASAF in MCH and Ethanol at Room Temperature

compound	solvent	λ_{em} [nm]	τ_3 [ns]:(A_3)	τ_2 [ns]:(A_2)	τ_1 [ns]:(A_1)	χ^2
FSF	MCH	410			**1.03**:(1)	1.06
		460			**1.03**:(1)	1.04
FASAF	MCH	410		**0.037**:(0.16)	**0.78**:(0.84)	1.07
		416		**0.037**:(−0.12)	**0.78**:(1)	1.09
		460		**0.037**:(−0.03)	**0.78**:(1)	1.06
FSF	EtOH	410	**0.011**:(0.48)	**0.043**:(0.32)	**1.81**:(0.2)	1.02
		430		**0.037**:(0.38)	**1.81**:(0.62)	1.02
		520		**0.033**:(−0.29)	**1.81**:(1)	1.06
		550		**0.037**:(−0.36)	**1.81**:(1)	1.09
FASAF	EtOH	410	**0.01**:(0.73)	**0.038**:(0.2)	**1.36**:(0.07)	1.02
		430		**0.032**:(0.57)	**1.36**:(0.43)	1.11
		520		**0.032**:(−0.31)	**1.36**:(1)	1.10
		550		**0.032**:(−0.45)	**1.36**:(1)	1.10

Independent analysis of decays collected at different emission wavelengths along the spectrum (from 400 to 550 nm) returns excellent fits with sums of two discrete exponential functions, with decay times of ca. 37 ps and 1.81 ns for **FSF** and 34 ps and 1.36 ns for **FASAF**. (See Table 1 and Figure 10.) In both compounds, the faster component appears as a decay time (positive amplitude) in the blue region of the spectrum and as a rise time (negative amplitude) at longer wavelengths. The longer component for **FSF** (1.81 ns) and **FASAF** (1.36 ns) appears always as a decay time and is longer for both compounds than the lifetime observed in MCH. Interestingly, the faster component has a similar order of

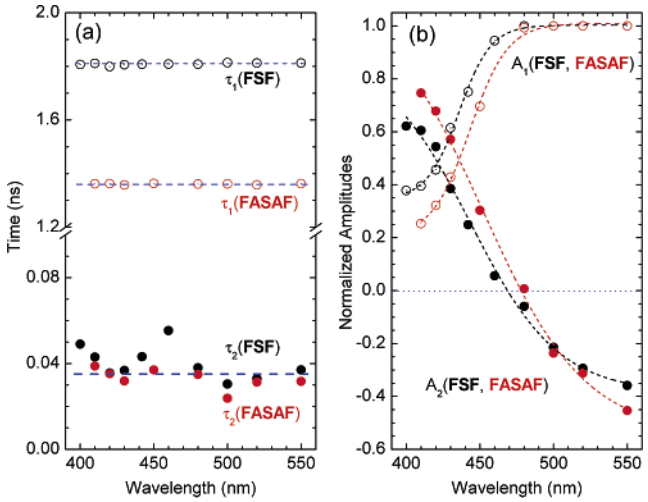

Figure 10. (a) Decay times and (b) amplitudes as a function of the observation wavelength, obtained from an independent single-wavelength analysis of fluorescence decays of **FSF** and **FASAF** in ethanol.

magnitude for **FSF** and **FASAF** in ethanol, as well as for **FASAF** in MCH, suggesting a common origin for this component but with a large fractional contribution for the overall decay in polar solvents.

In summary, the time-resolved fluorescence decays confirm the observations made from time-resolved emission spectra and indicate that (i) in nonpolar solvents, both **FSF** and **FASAF** emit from a state with a large LE contribution (referred to as a

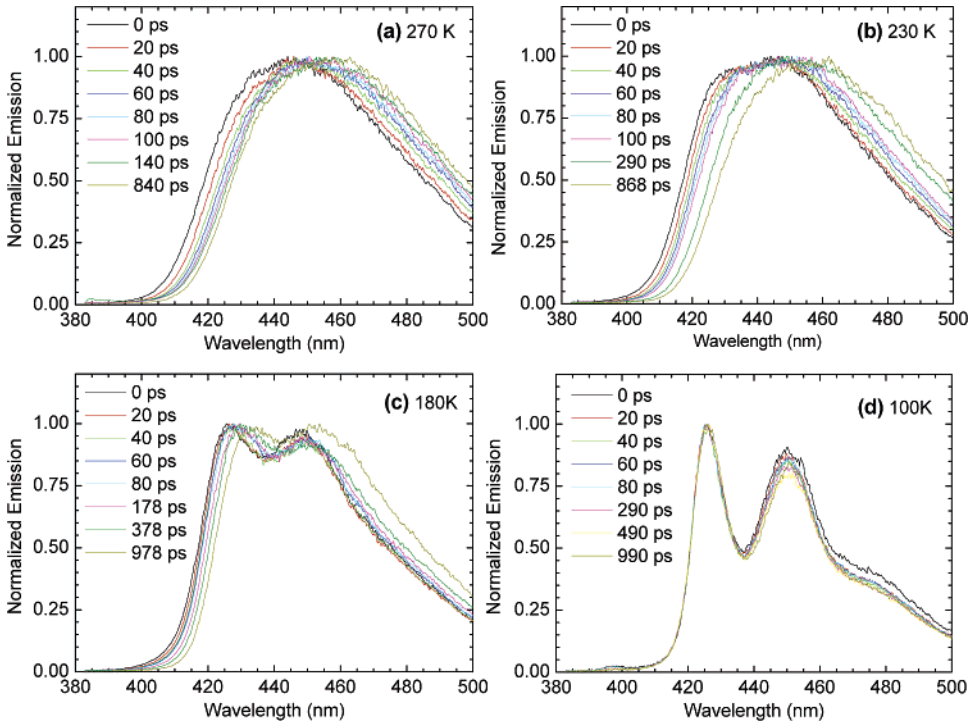

Figure 11. Normalized time-resolved emission spectra of **FASAF** in ethanol as a function of temperature: (a) 270, (b) 230, (c) 180, and (d) 100 K. $\lambda_{ex} = 375$ nm (see Figure S8 in Supporting Information for expanded spectra at the isoemissive points).

"LE-like" state in subsequent data analysis), (ii) **FASAF** in the nonpolar solvent (MCH) shows some conformational rearrangement during the excited state, (iii) in the polar solvent (ethanol), no LE-like emission is observed on the $t > 10$ ps time scale for both **FSF** and **FASAF**, suggesting that the emission is coming from a state with mainly CT character, which (iv) evolves in time, feeding a more relaxed CT state in about 40 ps.

An additional faster component of ~11 ps is observed for the fluorescence decays in ethanol when the emission is collected below 410 nm for **FSF** and below 420 nm for **FASAF** (Figure S7 in Supporting Information); for decays collected at longer wavelengths, this component is not detected (Table 1). The origin of this component is not clear, and because it appears only on the first two observed wavelengths, it is not shown in Figure 10. However, we note that the ~11 ps decay is not observed in MCH and that the spectral relaxation time of ethanol itself ($\tau_L = 12.4$ ps at room temperature)[30] coincides well with this component.

Time-Resolved Emission Spectra in Ethanol as a Function of Temperature. Time-resolved emission spectra of **FASAF** in ethanol collected at 270, 230, 180, and 100 K are shown in Figure 11. Decreasing the temperature strongly affects the spectrum. At 270 K, the behavior is similar to that at 290 K: the emission intensity decreases with time in the blue region of the spectrum and increases at longer wavelengths with an isoemissive point at 450 nm (Figure 11a). Note again that there is no evidence of emission from the LE-like state on the $t > 10$ ps time scale. Decreasing the temperature to 230 K clearly increases the relaxation time and induces the rapid appearance of a shoulder around 420 nm; as a consequence, the isoemissive point around 450 nm is lost (Figure 11b). On lowering the temperature to 180 K, the shoulder evolves to a resolved band at shorter wavelengths, and the isoemissive point is not observed (Figure 11c). Finally, at 100 K (below the melting point of ethanol), the relaxation process completely stops, and the emission spectrum becomes similar to that observed in nonpolar solvents (MCH or hexane) (Figure 11d).

The data shown in Figure 11 give clear evidence that above 230 K the emission on the $t > 10$ ps time scale comes from a CT state; in this temperature range, solvent reorganization occurs on a faster time scale, and emission directly from the LE-like state observed in nonpolar solvents simply cannot compete. The observed CT spectral relaxation indicates that large-amplitude motions of the molecule are involved in the formation of a more relaxed CT state, possibly increasing the average twist angle between the **F** and **S** units. Below 230 K, the solvent reorganization slows down, and the radiative decay of a state with mainly LE character starts to be competitive; as a consequence, the emission spectra below 230 K are a mixture of the emission observed in nonpolar and polar solvents, and the isoemissive point is lost. Finally, below the solvent melting point (159 K), the emission comes only from the state observed in nonpolar solvents with a large LE contribution, and no structural relaxation is observed.

Time-Resolved Fluorescence Decays as a Function of Temperature. Time-resolved fluorescence decays collected at 410 and 550 nm in ethanol were acquired between 290 and 220 K for **FASAF** and between 290 and 170 K for **FSF**. The results (decay times and amplitudes) obtained from independent analysis with a sum of discrete exponential functions are plotted as a function of temperature for **FSF** (Figure 12) and **FASAF** (Figure 13).

In agreement with the results obtained at room temperature, two main components were identified in the fluorescence decays for both **FSF** and **FASAF**. The slower component (τ_1), 1.81 ns for **FSF** and 1.36 ns for **FASAF** at 290 K, appears as a decay time (positive amplitude) at both emission wavelengths and is more important at 550 nm. Clearly, this component is connected with the CT relaxed excited-state lifetime (CT_R). The magnitude of this component starts to be independent of the emission wavelength, but on decreasing the temperature to around 230 K, different τ_1 values are obtained from fluorescence decays collected at 410 and 550 nm. Note that at 230 K the excitation spectra of **FSF** start to become dependent on the emission wavelength

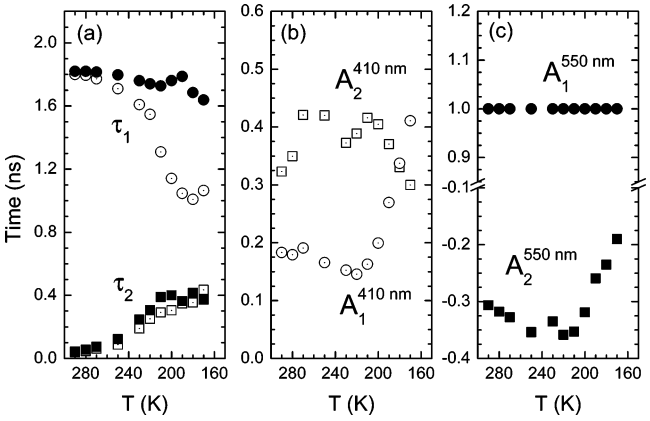

Figure 12. Results obtained from independent single-wavelength analysis of fluorescence decays of **FSF**, collected at 410 and 550 nm in an ethanol solution as a function of temperature: (a) (●, ■) decay times obtained at 410 nm, (○, □) decay times obtained at 550 nm; (b) amplitudes at 410 nm; and (c) amplitudes at 550 nm. At 410 nm, the decays are better described by a sum of three discrete exponential functions, and below 230 K (also at 550 nm), a three-exponential fit is used.

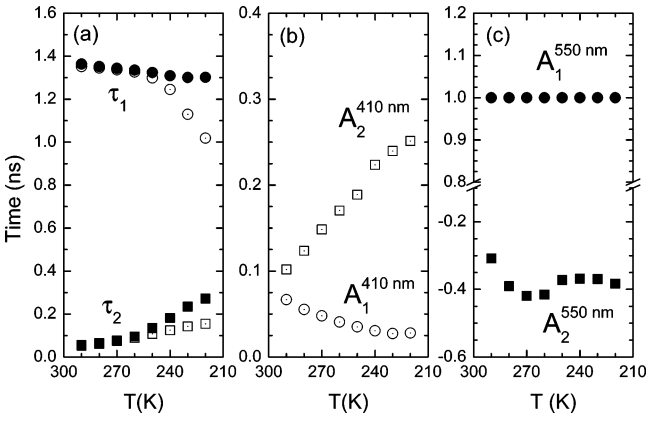

Figure 13. Results obtained from independent single-wavelength analysis of fluorescence decays of **FASAF**, collected at 410 and 550 nm in an ethanol solution as a function of temperature: (a) (●, ■) decay times obtained at 410 nm, (○, □) decay times obtained at 550 nm; (b) amplitudes at 410 nm; and (c) amplitudes at 550 nm. At 410 nm, the decays are better described by a sum of three discrete exponential functions, and below 230 K (also at 550 nm), a three-exponential fit is used.

(Figure 7) and LE-like emission starts to be observed in the time-resolved spectra (TRES). (See Figure 11b.) On further decrease in the temperature (to 170 K), the magnitude of τ_1 obtained from fluorescence decays collected at 410 nm matches the lifetime (~1 ns) of **FSF** in the nonpolar solvent (MCH). Similar behavior is suggested for **FASAF** from Figure 13.

The dependence of τ_1 on the observation wavelength is consistent with the observation of a REE[31] effect below 230 K and clearly shows the role of solvent relaxation in the stabilization of the CT state. At low temperatures, the radiative decay of the LE-like state starts to compete with the solvent relaxation time, and emission at higher energies is similar to the LE-like emission observed in nonpolar solvents. At 170 K, the effect is so pronounced that the emission collected at 410 nm decays with the lifetime observed in MCH.

The faster component (τ_2), ~40 ps at 290 K, for both **FASAF** and **FSF** appears as a decay time (positive amplitude) when the emission is collected at 410 nm and as a rise time (negative amplitude) when the emission is collected at 550 nm. This component is connected with the population of the relaxed

SCHEME 1

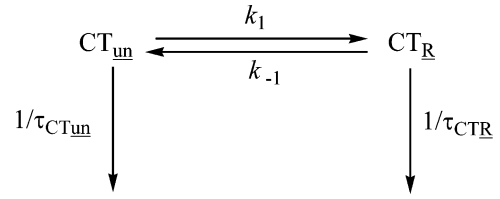

excited state emitting at longer wavelengths (CT_R). The high value found for this component at low temperatures (~400 ps) strongly supports the interpretation that large-amplitude motions, accompanying or following the charge redistribution in the excited state, are involved in the stabilization of the CT state. Note that this component is not significantly dependent on the observation wavelength, in agreement with it being connected with the structural stabilization of the CT state.

Again, an additional faster decay component (τ_3), with values between 8 ps at 290 K and 60 ps at 170 K, is detected in the fluorescence decays collected at 410 nm for both **FSF** and **FASAF**. Below 230 K, the decays collected at 550 nm are also better fitted with an additional faster component (~50 ps at 220 K). However, the fractional contribution of this component to the overall decay is very low: it is less than 5% at 410 nm and well below 0.3% at 550 nm, where it is absent at temperatures above 230 K (see Figures S1, S7, and S9 in Supporting Information). As mentioned above, the origin of this faster component is not understood, and clear experimental evidence to support the existence of a different kinetic species or the presence of a transient effect was not found. Triple-exponential decays have been reported before in systems showing dual fluorescence kinetics; the origin of such behavior has been interpreted in different ways, even for simpler structural systems such as DMABN[19,33,34] and related compounds. In the present case, the strong overlap of the LE-like and CT-like emission bands, the presence of a red-edge excitation effect that leads to a dependence of the slower decay component (τ_1) on the emission wavelength, and the low fractional contribution of the additional faster component (τ_3) make it particularly difficult to draw conclusions on its origin with any great certainty.

C. Data Analysis. The observation that no LE-like emission occurs in ethanol on the $t > 10$ ps time scale for the temperature range of 290−230 K strongly suggests that the relaxation of the CT state on this time scale and in this temperature range is due to the structural adaptation of the molecule to a new charge density distribution, meaning that the solvent and nuclear contributions for the CT-state stabilization are decoupled and that the molecular conformational change can be followed independently of the solvent reorganization. Additional support for this interpretation is given by the fact that the fluorescence decays at 550 nm are described by a sum of two discrete exponential functions in the temperature range of 290−220 K, suggesting that a "two-state" model ($CT_{unrelaxed} \rightarrow CT_{Relaxed}$) can describe the relaxation of the emissive CT state. Subsequent data analysis can then be undertaken and combined with the fluorescence decays collected at 550 nm to obtain information on the forward rate constant and energy activation barrier to the population of the relaxed CT state. (See Scheme 1.)

In Scheme 1, $\tau_{CT_{un}}$ represents the unrelaxed CT state (CT_{un}) lifetime, τ_{CT_R} represents the relaxed CT state (CT_R) lifetime, k_1 represents the forward rate constant, and k_{-1} represents the backward rate constant. The evolution with time of the CT_R emission is given by eq 1, where A_2 and A_1 represent the pre-exponential amplitudes and τ_1 and τ_2 are the two decay

components (Figures 12 and 13):

$$i_{CT}(t) = A_2 e^{-t/\tau_2} + A_1 e^{-t/\tau_1} \quad (1)$$

The solution of the differential equation describing the time evolution of the excited-state concentration of the two species represented in Scheme 1 leads to eq 2, which links the experimental observables τ_1 and τ_2 and the kinetic parameters

$$\frac{1}{\tau_{1,2}} = \frac{1}{2}[(X + Y) \mp ((X - Y)^2 + 4k_1k_{-1})^{1/2}] \quad (2)$$

where

$$X = k_1 + \frac{1}{\tau_{CT_{un}}} \quad (3)$$

and

$$Y = k_{-1} + \frac{1}{\tau_{CT_R}} \quad (4)$$

First, note that no significant changes in the steady-state emission spectra of **FSF** and **FASAF** (Figure 6) are observed between 290 and 220 K, meaning that a possible equilibrium between CT_{un} and CT_R is completely shifted to the CT_R product. Decreasing the temperature results in a decrease of both the forward and backward rate constants; this would lead to a variation of the ratio between CT_R and CT_{un} emissions. Second, the ratio A_2/A_1 at 410 nm is large and increases with the temperature decrease (Figures 12b, 13b), showing that the ratio k_1/k_{-1} increases with the temperature decrease.[27] Third, the temperature dependence of the longer component (τ_1) suggests that $k_{-1} \ll 1/\tau_{CT_R}$: if the backward reaction k_{-1} is important when compared with $1/\tau_{CT_R}$, then τ_1 would increase with decreasing temperature because k_{-1} decreases with the temperature decrease, and this is simply not observed (see Figures 12 and 13).

The above argument indicates that for both **FSF** and **FASAF** in the temperature range studied the condition $k_{-1} \ll 1/\tau_{CT_R}$ is valid; consequently, eq 2 can be rewritten in the form

$$\tau_1 = \tau_{CT_R} \quad (5)$$

and

$$\frac{1}{\tau_2} = k_1 + \frac{1}{\tau_{CT_{un}}} \quad (6)$$

The forward rate constant can easily be determined from eq 6, assuming that $1/\tau_{CT_{un}}$ is small when compared with $1/\tau_2$. This is a reasonable assumption, because the lifetimes of the LE-like and CT-like emissions are both much larger than τ_2. Figure 14a, b represents the Arrhenius plots of the rate constant k_1 for **FSF** and **FASAF**, respectively. Good linear relationships are observed in both cases, from which the magnitudes of k_1(**FSF**) $= (21.4 \pm 4.5) \times 10^9$ s^{-1} and k_1(**FASAF**) $= (18.5 \pm 5.9) \times 10^9$ s^{-1} (at 290 K) and the activation energy barriers, E_a(**FSF**) $= 3.98 \pm 0.11$ kcal mol^{-1} and E_a(**FASAF**) $= 3.84 \pm 0.16$ kcal mol^{-1}, have been determined; these values are close to the energy barrier for viscous flow in ethanol[35] (3.54 kcal mol^{-1}), lending additional support to the interpretation that the reaction is controlled by large-amplitude motions between the **F** and **S** moieties.

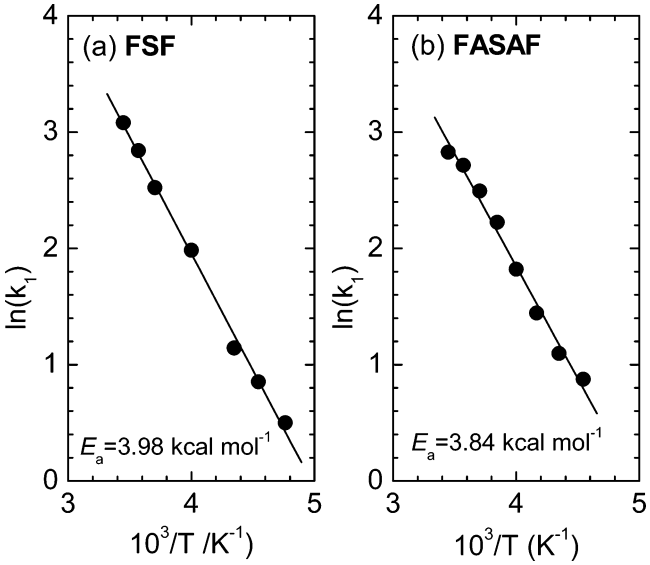

Figure 14. Arrhenius plots of the forward CT rate constant k_1 of (a) **FSF** and (b) **FASAF**. The activation energies E_a, calculated from the fitting parameters with the expression $k_1 = k_0 \exp(-E_a/RT)$, are given in each plot.

IV. Conclusions

A strong solvatochromic effect has been observed for both **FSF** and **FASAF** in polar solvents with dual fluorescence detected in polar solvents at low temperatures in ethanol. From the solvatochromism and thermochromism of both compounds, we have deduced that these molecules, in their excited states, undergo an intramolecular charge-transfer reaction stabilized by the solvent polarity and accompanied/followed by molecular structural changes.

The kinetics of the structural rearrangement of **FSF** and **FASAF** in the excited state has been followed in ethanol in the 290−220 K temperature range using time-resolved fluorescence techniques, and the rate constant (k_1(20 °C) $\approx 20 \times 10^9$ s^{-1}) and energy activation barrier ($E_a \approx 3.9$ kcal mol^{-1}) were determined for both compounds.

The magnitudes of the forward rate constant (k_1) and the energy barriers (E_a) obtained are slightly larger than the energy barrier for viscous flow in ethanol (3.54 kcal mol^{-1}), showing that the population of the final relaxed (CT_R) state is controlled by large-amplitude motions occurring during the excited state of the molecule; an indication is obtained that these could be the reorganization of **S** and **F** units to a highly twisted CT excited-state conformation, by analogy to a TICT model. Further clarification of this point should be provided by a planned study of the $CT_{un} \rightarrow CT_R$ reaction in **F/S**-type oligomers that possess rigid planar and sterically crowded twisted conformations.

Acknowledgment. This work was funded by One North-East via the County Durham Sub-regional Partnership, project S.P./082, and the nanotechnology UIC project, and by CEN-AMPS via the Photonic Materials Institute. We also thank EPSRC for funding this work in the chemistry department through the ESF Eurocores SONS Program. I.I.P. thanks M.R.B. for the opportunity to visit the University of Durham.

Supporting Information Available: Chemical synthesis of **S** and **FF**, absorption spectra of **FSF** in hexane−ethanol mixtures, emission spectra collected with different excitation wavelengths and in different solvents, time-resolved spectra, and fluorescence decays. This material is available free of charge via the Internet at http://pubs.acs.org.

References and Notes

(1) Burroughes, J. H.; Bradley, D. D. C.; Brown, A. R.; Marks, R. N.; Mackay, K.; Friend, R. H.; Burn, P. L.; Holmes, A. B. *Nature* **1990**, *347*, 539−541.

(2) (a) Kraft, A.; Grimsdale, A. C.; Holmes, A. B. *Angew. Chem., Int. Ed.* **1998**, *37*, 402−428. (b) Mitschke, U.; Bäuerle, P. *J. Mater. Chem.* **2000**, *10*, 1471−1507. (c) Perepichka, I. F.; Perepichka, D. F.; Meng, H.; Wudl, F. *Adv. Mater.* **2005**, *17*, 2281−2305.

(3) Akcelrud, L. *Prog. Polym. Sci.* **2003**, *28*, 875−962.

(4) Scherf, U.; List, E. J. W. *Adv. Mater.* **2002**, *14*, 477−487.

(5) Neher, D. *Macrom. Rapid Commun.* **2001**, *22*, 1365−1385.

(6) (a) Grell, M.; Bradley, D. D. C. *Adv. Mater.* **1999**, *11*, 895−905. (b) Lupton, J. M.; Koeppe, R.; Müller, J. G.; Feldmann, J.; Scherf, U.; Lemmer, U. *Adv. Mater.* **2003**, *15*, 1471−1474. (c) Forrest, S. *Org. Electron.* **2003**, *4*, 45−48.

(7) (a) Brédas, J.-L.; Beljonne, D.; Coropceanu, V.; Cornil, J. *Chem. Rev.* **2004**, *104*, 4971−5003. (b) Pron, A.; Rannou, P. *Prog. Polym. Sci.* **2002**, *27*, 135−190.

(8) (a) Leclerc, M. *Adv. Mater.* **1999**, *11*, 1491−1498. (b) McQuade, D. T.; Pullen, A. E.; Swager, T. M. *Chem. Rev.* **2000**, *100*, 2537−2574.

(9) D'Andrade, B. W.; Forrest, S. R. *Adv. Mater.* **2004**, *16*, 1585−1595.

(10) (a) Bernius, M. T.; Inbasekaran, M.; O'Brien, J.; Wu, W. *Adv. Mater.* **2000**, *12*, 1737−1750. (b) Leclerc, M. *J. Polym. Sci., Part A: Polym. Chem.* **2001**, *39*, 2867−2873. (c) Knaapila, M.; Stepanyan, R.; Lyons, B.; Torkelli, M.; Monkman, A. P. *Adv. Funct. Mater.* **2006**, *16*, 599−609.

(11) Redecker, M.; Bradley, D. D. C.; Inbasekaran, M.; Woo, E. P. *Appl. Phys. Lett.* **1998**, *73*, 1585−1587. (b) Redecker, M.; Bradley, D. D. C.; Inbasekaran, M.; Woo, E. P. *Appl. Phys. Lett.* **1999**, *74*, 1400−1402. (c) Sirringhaus, H.; Wilson, R. J.; Friend, R. H.; Inbasekaran, M.; Wu, W.; Woo, E. P.; Grell, M.; Bradley, D. D. C. *Appl. Phys. Lett.* **2000**, *77*, 406−408.

(12) Yang, L.; Feng, J.; Liao, Y.; Ren, A. *Polymer* **2005**, *46*, 9955−9964.

(13) (a) Romaner, L.; Pogantsch, A.; Scandiucci de Freitas, P.; Scherf, U.; Gaal, N.; Zojer, E.; List, E. J. W. *Adv. Funct. Mater.* **2003**, *13*, 597−601. (b) Li, J. Y.; Ziegler, A.; Wegner, G. *Chem.−Eur. J.* **2005**, *11*, 4450−4457. (c) Lim, S.-F.; Friend, R. H.; Rees, I. D.; Li, J.; Ma, Y.; Robinson, K.; Holmes, A. B.; Hennebicq, E.; Beljonne, D.; Cacialli, F. *Adv. Funct. Mater.* **2005**, *15*, 981−988. (d) Dias, F. B.; Maiti, M.; Hintschich, S. I.; Monkman, A. P. *J. Chem. Phys.* **2005**, *122*, 54904. (e) Dias, F. B.; Knaapila, M.; Burrows, H.; Monkman, A. P. *Macromolecules* **2006**, *39*, 1598−1606.

(14) Perepichka, D. F.; Perepichka, I. F.; Meng, H.; Wudl, F. In *Organic Light-Emitting Materials and Devices*; Li, Z. R., Meng, H., Eds.; CRC Press: Boca Raton, FL, 2006; Chapter 2, pp 45−293.

(15) (a) Sonar, P.; Zhang, J.; Grimsdale, A. C.; Müllen, K.; Surin, M.; Lazzaroni, R.; Leclère, P.; Tierney, S.; Heeney, M.; McCulloch, I. *Macromolecules* **2004**, *37*, 709−715. (b) Cho, N. S.; Hwang, D.-H.; Jung, B.-J.; Lim, E.; Lee, J.; Shim, H.-K. *Macromolecules* **2004**, *37*, 5265−5273. (c) Ding, J.; Day, M.; Robertson, G.; Roovers, J. *Macromolecules* **2002**, *35*, 3474−3483. (d) Donat-Bouillud, A.; Lévesque, I.; Tao, Y.; D'Iorio, M.; Beaupré, S.; Blondin, P.; Ranger, M.; Bouchard, J.; Leclerc, M. *Chem. Mater.* **2000**, *12*, 1931−1936.

(16) (a) Hou, Q.; Zhou, Q.; Zhang, Y.; Yang, W.; Yang, R.; Cao, Y. *Macromolecules* **2004**, *37*, 6299−6305. (b) Hou, Q.; Xu, Y.; Yang, W.; Yuan, M.; Peng, J.; Cao, Y. *J. Mater. Chem.* **2002**, *12*, 2887−2892. (c) Cho, N. S.; Hwang, D.-H.; Lee, J.-I.; Jung, B.-J.; Shim, H.-K. *Macromolecules* **2002**, *35*, 1224−1228.

(17) Morgado, J.; Charas, A.; Martinho, J.; Alcácer, L. *Synth. Metals* **2005**, *154*, 81−84.

(18) Perepichka, I. I.; Perepichka, I. F.; Bryce, M. R.; Pålsson, L.-O. *Chem. Commun.* **2005**, 3397−3399.

(19) Grabowski, Z. R.; Rotkiewicz, K.; Rettig, W. *Chem. Rev.* **2003**, *103*, 3899−4031.

(20) Acheson, R. M.; Stubbs, J. K. *J. Chem. Soc., Perkin Trans. 1* **1972**, *1*, 899−903.

(21) (a) Koizumi, Y.; Seki, S.; Acharya, A.; Saeki, A.; Tagawa, S. *Chem. Lett.* **2004**, *33*, 1290−1291. (b) Lee, S. H.; Tsutsui, T. *Thin Solid Films* **2000**, *363*, 76−80. (c) Jo, J.; Chi, C.; Höger, S.; Wegner, G.; Yoon, D. Y. *Chem.−Eur. J.* **2004**, *10*, 2681−2688. (b) Geng, Y.; Trajkovska, A.; Katsis, D.; Ou, J. J.; Culligan, S. W.; Chen, S. H. *J. Am. Chem. Soc.* **2002**, *124*, 8337−8347. (d) Belletête, M.; Beaupé, S.; Bouchard, J.; Blondin, P.; Leclerc, M.; Durocher, G. *J. Phys. Chem. B* **2000**, *104*, 9118−9125.

(22) Lee, S. H.; Nakamura, T.; Tsutsui, T. *Org. Lett.* **2001**, *3*, 2005−2007.

(23) Beechem, J. M.; Gratton, E. *Proc. SPIE* **1988**, *909*, 70−81.

(24) Cornil, J.; Gueli, I.; Dkhissi, A.; Sancho-Garcia, J. C.; Hennebicq, E.; Calbert, J. P.; Lemaur, V.; Beljonne, D.; Brédas, J. L. *J. Chem. Phys.* **2003**, *118*, 6615−6623.

(25) Herbich, J.; Kapturkiewicz, A. *J. Am. Chem. Soc.* **1998**, *120*, 1014−1029.

(26) Anémian, R.; Mulatier, J.-C.; Andraud, C.; Stéphan, O.; Vial, J.-C. *Chem. Commun.* **2002**, 1608−1609.

(27) (a) Zachariasse, K. A.; Grobys, M.; Tauer, E. *Chem. Phys. Lett.* **1997**, *274*, 372−382. (b) Yoshihara, T.; Druzhinin, S. I.; Demeter, A.; Kocher, N.; Stalke, D.; Zachariasse, K. *J. Phys. Chem A* **2005**, *109*, 1497−1509. (c) Il'ichev, Y. V.; Kuhnle, W.; Zachariasse, K. A. *J. Phys. Chem. A* **1998**, *102*, 5670−5680. (d) Yoshihara, T.; Druzhinin, S. I.; Zachariasse, K. A. *J. Am. Chem. Soc.* **2004**, *126*, 8535−8539.

(28) Zachariasse, K. A. *Chem. Phys. Lett.* **2000**, *320*, 8−13.

(29) (a) Tominaga, K.; Walker, G. C.; Jarzeba, W.; Barbara, P. F. *J. Phys. Chem.* **1991**, *95*, 10475−10485. (b) Tominaga, K.; Walker, G. C.; Kang, T. J.; Barbara, P. F.; Fonseca, T. *J. Phys. Chem.* **1991**, *95*, 10475−10485.

(30) *Principles of Fluorescence Spectroscopy*, 2nd ed.; Lakowicz, J. R., Ed. Kluwer Academic/Plenum Publishers: New York, 1999.

(31) (a) Demchenko, A. P. *Luminescence* **2002**, *17*, 19−42. (b) Itoh, K.; Azumi, T. *J. Chem. Phys.* **1975**, *62*, 3431−3438. (c) Azumi, T.; Itoh, K.; Shiraishi, H. *J. Chem. Phys.* **1976**, *65*, 2550−2555.

(32) Dias, F. B.; Maçanita, A. L.; Melo, J. S.; Burrows, H. D.; Güntner, R.; Scherf, U.; Monkman, A. P. *J. Chem. Phys.* **2003**, *118*, 7119−7126.

(33) Zachariasse, K. A.; Yoshihara, T.; Druzhinin, S. I. *J. Phys. Chem. A* **2002**, *106*, 6325−6333.

(34) Dahl, K.; Biswas, R.; Ito, N.; Maroncelli, M. *J. Phys. Chem. B* **2005**, *109*, 1563−1585.

(35) Das, K.; Ashby, K. D.; Wen, J.; Petrich, J. W. *J. Phys. Chem. B* **1999**, *103*, 1581−1585.